Communications Medicine

https://doi.org/10.1038/s43856-026-01785-2

Article in Press

Observational in vivo axon development during early childhood in autism spectrum disorder and developmental disability using MRI

Received: 25 March 2025

Accepted: 2 July 2026

Published online: 22 July 2026

Cite this article as: Liu, Y., Zhang, J., Rolls, E.T. *et al.* Observational in vivo axon development during early childhood in autism spectrum disorder and developmental disability using MRI. *Commun Med* (2026). https://doi.org/10.1038/s43856-026-01785-2

Yuqi Liu, Jiaying Zhang, Edmund T. Rolls, Yuan Dai, Shujie Geng, Lin Deng, Zilin Chen, Yue Zhang, Yunjun Sun, Wei Zhou, Lingli Zhang, Tai Ren, Jianfeng Feng, Miao Cao & Fei Li

Observational *in vivo* axon development during early childhood in autism spectrum disorder and developmental disability using MRI

Yuqi Liu[1,2†], Jiaying Zhang[3,4†*], Edmund T. Rolls[5,6,7], Yuan Dai[1], Shujie Geng[4,5], Lin Deng[1], Zilin Chen[1], Yue Zhang[4,5], Yunjun Sun[1], Wei Zhou[1],Lingli Zhang[1], Tai Ren[1], Jianfeng Feng[4,5], Miao Cao[1,4,5*], Fei Li[1*]

[1]Developmental and Behavioral Pediatric Department and Child Primary Care Department, Ministry of Education-Shanghai Key Laboratory for Children's Environmental Health, Xinhua Hospital, Shanghai Jiao Tong University School of Medicine; Shanghai 200092, China.

[2]Center of Psychosomatic Medicine, Sichuan Provincial Center for Mental Health, Sichuan Provincial People's Hospital, University of Electronic Science and Technology of China, Chengdu, China.

[3]School of Artificial Intelligence, Beijing University of Posts and Telecommunications; Beijing 100876, China.

[4]Key Laboratory of Computational Neuroscience and Brain-Inspired Intelligence (Fudan University), Ministry of Education; Shanghai, China.

[5]Institute of Science and Technology for Brain-Inspired Intelligence, Fudan University; Shanghai 200433, China.

[6]Department of Computer Science, University of Warwick; Coventry CV4 7AL, UK.

[7]Oxford Centre for Computational Neuroscience; Oxford, UK.

***Corresponding authors**

Fei Li: feili@shsmu.edu.cn

Miao Cao: mcao@fudan.edu.cn

Jiaying Zhang: jiaying.zhang@bupt.edu.cn

†These authors contributed equally to this work.

Abstract

Background

Elucidating the altered spatiotemporal development of white matter (WM) axons during early childhood is essential for uncovering the neuropathology of autism spectrum disorder (ASD). However, previous studies have often failed to account for the heterogeneity of developmental trajectories or to adequately control for co-occurring developmental delay/intellectual disability (DD/ID), limiting our understanding of whether ASD-related alterations represent qualitative deviations or quantitative delays in otherwise preserved maturational patterns.

Methods

We analyzed multi-shell diffusion MRI and behavioral data from 364 children aged 1–7 years, (156 individuals with ASD, 48 individuals with DD/ID), and 160 typically developing (TD) controls) using the Neurite Density Index (NDI)—an MRI-derived marker of axonal density. A subset of ASD children also underwent longitudinal MRI scans and provided blood metabolic and protein profiles.

Results

We identified the same three WM clusters in both typical and atypical development. These clusters exhibit distinct developmental stages with successively decreasing growth rates in ASD, similar to TD but delayed overall, especially for ASD with DD/ID, while DD/ID display little developmental effect. These findings are further validated across split-half, male-only and longitudinal subdataset. Furthermore, we found NDIs of these WM clusters in ASD are: a) correlated with cognitive impairments at the stage with a fast developmental pace and social deficits at the stage with a moderate-slow developmental pace; b) linked with multiple metabolic and protein measurements.

Conclusions

ASD children exhibit the same coordinated spatial pattern of white matter development as TD, but with distinct developmental trajectories. These findings advance our understanding of the neuropathological underpinnings of ASD heterogeneity in early childhood, and highlight potential targets for future therapeutic design and evaluation.

Plain language summary

Autism Spectrum Disorder (ASD) is a neurodevelopmental disorder that begins early in life, characterized by social and cognitive deficits. However, we know little about how white matter – the fiber nerves connecting different brain areas - develops differently in young ASD children. Here, we use non-invasive MRI scans of 364 children aged 1 to 7 years, including children with typical development and ASD children with or without developmental delay/intellectual disability, to estimate how densely packed the nerve fibers were in core white matter. We found the overall pattern of white matter development – where and how these changes appeared across the brain – was similar across groups, but the timing and rate of development differed in children with ASD. And these white matter differences were also linked to behavior and blood-based metabolic and protein markers.

Introduction

Autism spectrum disorder (ASD), a typical neurodevelopmental disorder (NDD)[1], manifests from early childhood with symptoms such as poor acquisitions of general cognitive abilities and reduced interest in social activities[2]. The cognitive impairments in ASD are exacerbated when co-occuring with developmental delay/intellectual disability (DD/ID)[2]. The symptoms observed in ASD and DD/ID suggest underlying functional deficits in the brain, which may be linked to atypical white matter development during this critical life period. As axons represent a key microstructural component of white matter, axon development in early childhood could be pivotal in understanding the neurophysiology of ASD. Although cognitive impairment is widely recognized as a critical factor in ASD research, most of previous studies merely accounted for intellectual disability of ASD using development quotient (DQ)/ intelligence quotient (IQ) as covariates in statistical models or selection criteria. Moreover, we found that very few studies have explicitly accounted for the intellectual disability as a co-occurring condition of ASD with DD/ID, by including four distinct groups: typically developing (TD) children, children with ASD and DD/ID, children with ASD without DD/ID, and children with DD/ID alone as disease controls. Naturally, a series of critical questions arise: What are the specifically altered maturation patterns of white matter microstructure during early childhood in ASD compared to TD and DD/ID children? What are the associations between these alterations and their clinical implications?

Previously, altered white matter axon density in ASD were identified only in postmortem studies, exemplified by lower axon numbers and smaller axon sizes in the corpus callosum (CC)[3]. Despite providing invaluable information on the neuropathology of ASD, these studies had inherent limitations, such as the scarcity of brain samples from young children, the absence of information on donors' behavioral profiles

and so on. In contrast, diffusion MRI provides a non-invasive window for quantifying *in vivo* white matter microstructure. In particular, using diffusion tensor imaging (DTI), ASD and DD/ID children exhibited reduced fractional anisotropy (FA) with flatter developmental trajectories in white matter tracts compared with TD children[4-7]. These findings suggest the presence of atypical white matter growth in individuals with ASD and DD/ID. However, DTI metrics lack specificity for tissue properties[8]. For example, FA can be affected by factors such as the axon packing density and the spatial coherence of axon alignments. Therefore, changes in FA may not necessarily be linked to alterations in specific axon morphological features[9].

Neurite orientation dispersion and density imaging (NODDI)[10] provides tissue-specific quantifications of white matter microstructure by exploiting biophysical models to disentangle the water diffusion of each voxel into multiple compartments. Histologically validated NODDI metrics - including the neurite density index (NDI) and orientation dispersion index (ODI)) - represent axon density and the spatial coherence of axon alignments in white matter respectively[11]. Previous neurodevelopmental studies using NODDI revealed that the white matter NDI was sensitive to developmental processes[12]. For instance, the NDI of the entire white matter increased with age in TD, characterized by an initial rapid growth followed by a more gradual increase[12-14]. Furthermore, the maturation curves of NDI in TD exhibited spatial heterogeneity across the cerebral white matter, e.g., the earlier development of callosal fibers than the association and projection tracts[12]. In ASD adults without cognitive impairment (i.e., ASD without DD/ID), aberrant NDI values have been linked to clinical symptomatology[15-18]. However, previous diffusion MRI studies in ASD have largely relied on cross-sectional designs and traditional DTI metrics, often focusing on linear trajectories or single tracts while excluding minimally verbal individuals and those with developmental delay or intellectual disability. As a result, the early development of microstructurally specific metrics such

as NDI in this heterogeneous population remains largely unexplored. Given evidence that white matter alterations in ASD are widespread and strongly age-dependent—potentially preceding observable behavioral signs[19,20]—it has been hypothesized that ASD may preserve the coordinated spatial organization of white matter axon development while exhibiting distinct temporal trajectories. Yet, due to the challenges of acquiring multi-shell diffusion MRI data in young children, this spatiotemporal pattern of axonal development during early childhood has not been systematically characterized in ASD.

To answer these questions, we employ a multifaceted dataset of multi-shell diffusion MRI and comprehensive behavior assessments in 364 children under 8 years old, including 156 individuals with ASD (105 with DD/ID and 51 without DD/ID), 160 TD participants and 48 individuals with DD/ID. Based on the functional segmentation of white matter, we hypothesized that the developmental trajectories of axon density (NDI) are not uniform across the brain. Specifically, we predicted that white matter fibers would cluster into distinct spatiotemporal modules with divergent maturation patterns, and that deviations from normative trajectories in ASD would depend on both the specific module and the child's functional level (ASD with vs. without DD/ID). To test these hypotheses, we first delineated the coordinated spatial organization of axon development in early childhood by performing hierarchical clustering of NDI across the core white matter, identifying three distinct white matter clusters. We then modeled the developmental trajectories of NDI within each cluster using generalized additive models (GAM)[21], and subsequently derived growth rates from the first derivatives to define distinct developmental stages (fast, moderate, and slow). These findings were validated using split-half replication, male-only subsample analyses, and a longitudinal subsample. To establish clinical relevance, we examined correlations between cluster-wise NDI and behavioral measures in children with atypical development. Finally, given accumulating evidence

of metabolic and protein dysregulation in ASD[22-24], we conducted exploratory analyses linking white matter NDI to peripheral blood metabolic and protein profiles in a subset of participants, aiming to elucidate potential interactions between brain microstructure and systemic physiology in ASD (Fig. 1).

Methods and Materials

Participants

A total of 404 participants under 8 years old were recruited in the neurodevelopmental project - Shanghai Autism Early Development Cohort (SAED)[25] in Xinhua Hospital affiliated to Shanghai Jiao Tong University. After MR image quality control, a total of 40 participants were excluded after MR image quality control (see next subsection - Multi-shell diffusion MRI acquisition, quality control and processing for more details) and 364 children were included in early childhood, comprising 156 children diagnosed as ASD (105 with DD/ID and 51 without DD/ID), 48 children with DD/ID and 160 age-matched TD children. All participants had no contraindications for MRI, no suspected vision or hearing problems or known genetic disorders and no neurological conditions. Clinical diagnoses were made by experienced clinicians based on the Diagnostic and Statistical Manual of Mental Disorders-Fifth Edition (DSM-5)[1] and were confirmed using the age-appropriate modules of the Autism Diagnostic Observation Schedule (ADOS)[26] - specifically, the standard ADOS module 1 for children over 30 months of age and the ADOS Toddler Module for those between 12 and 30 months. None of the children diagnosed before 30 months of age had any change in diagnosis during subsequent follow-up visits. The ADOS calibrated severity scores, including the social affect calibrated severity score (SA-CSS) and the restricted and repetitive behaviors calibrated severity score (RRB-CSS), were calculated to allow the comparison of autism severity across participants

tested with different ADOS modules[27]. The neurocognitive assessments were made around their first MRI visit. The DQ was assessed by the Gesell Developmental Schedules (GDS)[28] for children younger than 4 years. The IQ was assessed by the Wechsler Preschool and Primary Scale of Intelligence (WPPSI)[29] for 4- to 6-year-old children and the Wechsler Intelligence Scale for Children-Revised (WISC-R)[30] for children older than 6 years. The Childhood Autism Rating Scale (CARS)[31] and Social Responsiveness Scale (SRS)[32] were used to assess social-related clinical phenotypes. All participants had no neurological issues, such as suspected vision problems, hearing problems, known genetic disorders or neurological conditions. Informed consent was obtained from the parents or the guardians of each participant. The study was conducted in accordance with the Declaration of Helsinki, with approval from the Ethical Committee of the Xinhua Hospital Affiliated to Shanghai Jiao Tong University, and in compliance with all applicable laws and regulations. All necessary biosecurity and institutional safety protocols were followed during the study.

Multi-shell diffusion MRI acquisition, quality control and processing

Multi-shell diffusion-weighted MRI scans were performed on a 3.0T Siemens Verio MRI scanner with a 32-channel coil in the Shanghai International Medical Centre. An echo-planar imaging (EPI) sequence was employed, and its parameters were as follows: 65 axial slices; echo time (TE) = 84 ms; repetition time (TR) = 14500 ms; field of view (FOV) = 192 mm × 192 mm; voxel size = 2×2×2 mm^3; two shells with diffusion weighting of b=1000 and 2000 s/mm^2; 30 directions for each shell; 3 additional b0 images without diffusion weighting (b = 0 s/mm^2); a posterior-to-anterior phase-encoding direction; a full k-space acquisition; and a total acquisition time ~ 15 minutes. Children with poor compliance received chloral hydrate sedation by experienced nurses, a common practice for pediatric MR examinations.

The image quality of diffusion MR images was visually checked to ensure image quality in this study by two researchers who were blinded to the diagnosis (Dr. J Zhang and Dr. Y Liu). We assessed the diffusion-weighted MR images carefully from the following aspects: 1) the coverage of cerebral regions (occipital/parietal/temporal/frontal lobes) was complete; 2) signal dropout due to head motion or zig-zag patterns had occurred; and 3) zipper artefacts[33], the most common equipment artefacts, were caused by radio frequency (RF) break-through (Supplementary Fig. 1). Images were excluded if they met the following exclusion criteria: 1) more than 3 volumes (more than 5% of all volumes) that exhibited signal dropout, zig-zag patterns and/or zipper artefacts; and 2) incomplete coverage of the 36 selected core white matter ROIs. After image quality control, a total of 40 participants were excluded, including 16 individuals with ASD with DD/ID, 5 individuals with ASD without DD/ID, 17 TD participants and 2 DD/ID participants.

Diffusion-weighted MR images were preprocessed using MRtrix3[34] (www.mrtrix.org) and FSL (FMRIB Software Library)[35] version 6.0.6 (https://fsl.fmrib.ox.ac.uk/fsl/fslwiki/FSL). The preprocessing steps were as follows: 1) denoising[36]; 2) removing the Gibbs ring[37]; 3) eddy-current distortion and motion correction using the FSL eddy[38]; and 4) B1 bias correction using the Ants algorithm[39]. After preprocessing, we computed DTI and NODDI metrics in the native space using FSL and in-house scripts with the NODDI MATLAB toolbox (https://www.nitrc.org/projects/noddi_toolbox), respectively. To minimize the potential bias that may be introduced by inaccurate registrations in early childhood, we defined the core white matter ROI masks using the following multi-level computational framework: 1) we first warped the labels of ICBM-DTI-81 white matter atlas[40] (representing the core white matter ROIs across the brain) into the study-specific group tensor template; 2) we then multiplied the masks of the core white matter ROIs and the white matter skeleton of the whole sample; and 3) finally, we warped the labels of the skeletonized core white

matter ROIs into study-specific age-specific tensor templates (one per year, seven in total). Due to incomplete coverage of the cerebellum, we chose only 36 core white matter ROIs in the cerebrum (Supplementary Table 1).

Seven age-specific tensor templates were created from tensor maps of a selective subset of participants within the same year. We selected 5 to 6 children in the ASD subgroups and TD group per year with excellent image quality (Supplementary Table 2). Then, the group-specific tensor template was created using these seven age-specific tensor templates and was further used to create the white matter skeleton of the whole sample. The registrations involved were conducted using NiftiReg (http://cmictig.cs.ucl.ac.uk/wiki/index.php/NiftyReg)[41] and DTI-TK (Diffusion Tensor Imaging ToolKit, https://dti-tk.sourceforge.net)[42]. Notably, we chose skeletonized core white matter ROIs here to 1) minimize the potential bias of inaccuracies in registration and 2) avoid the influences of subjective experience on white matter anatomy. For all the participants, their NDI maps were transformed from the native space into the space of the corresponding study-specific age-specific tensor template. The transformation matrix was estimated by registering the tensor maps from the native space into the study-specific, age-specific tensor template. Finally, for all the participants, we computed the mean NDI value of the 36 core white matter ROIs for the following statistical analyses.

Metabolomics and proteomics blood measurements

We measured 302 blood metabolites using liquid chromatography-mass spectrometry and 1455 proteins through label-free data-independent acquisition, with all measurements subsequently normalized (Supplementary Data 2 and Supplementary Data 3).

Plasma samples were collected from peripheral blood by centrifugation, aliquoted, and stored at -80°C. For extraction, 50μL of thawed plasma was deproteinized using an acetonitrile-methanol (1:1, v/v) solution containing isotopically-labeled internal standards. The mixture underwent vortexing, sonication, and incubation at -40°C, followed by centrifugation at 12,000 rpm. The resulting supernatant was dried under nitrogen, reconstituted in 60% acetonitrile, and centrifuged again to remove particulates. The final supernatant was transferred to vials for analysis. Quality control (QC) samples, created by pooling aliquots from all study samples, were prepared and analyzed alongside the experimental samples to monitor system stability.

Metabolite profiling was conducted using a targeted multi-reaction monitoring (MRM) method on a UPLC-MS/MS platform[43]. Chromatographic separation was achieved on a Waters Atlantis Premier BEH Z-HILIC Column（1.7 μm, 2.1 mm *150 mm）using a gradient of (A) 8:2 water: acetonitrile and (B) 1:9 water: acetonitrile, both containing 10 mmol/L ammonium acetate (pH 9.0). The analysis was performed on an AB Sciex QTrap 6500 plus mass spectrometer operating in both positive (+5000V) and negative (-4500V) ion modes. Key ion source parameters included a temperature of 500°C and curtain and nebulizer gas pressures set to 35 psi and 50 psi, respectively.

Raw LC-MS/MS data were processed with SCIEX Analyst and Data Driven Flow (v-1.0.1) software for peak integration and metabolite quantification. The resulting data matrix was subjected to a rigorous preprocessing pipeline: metabolites with poor detection rates (<80%) were filtered out, and data were normalized using Probabilistic Quotient Normalization (PQN) to correct for analytical variance. Subsequently, the data underwent log transformation and auto-scaling to prepare for statistical analysis. The

high quality and reproducibility of the dataset were confirmed by the tight clustering of QC samples in a Principal Component Analysis (PCA).

Statistics and Reproducibility

Clustering analyses

To reveal the spatial pattern of early white matter development, we conducted hybrid hierarchical clustering analysis[44] (implemented in the "hybridHclust" package in R version 3.6.0) using the mean NDI value of the 36 core white matter regions into clusters for all four groups. . For each group, the optimal number of clusters was chosen as the “knee point” on the inter-cluster distance vs. the number of cluster plots.

Modelling developmental curves, calculating growth rates and defining developmental stages

Inspired by the nonlinear nature of white matter development[45], we modelled developmental curves of NDI in each white matter cluster using a nonparametric regression approach — generalized additive model (GAM)[21] with sex and head motion as covariates ("mgcv" package in R4.2.1). Here, sex and head motion during the MR scan were included in the GAM as covariates, using the following formula:

$$\mathbf{y_{i(age)} \sim \beta_0 + s(age) + \beta_1 * sex + \beta_2 * AMzscore + \beta_3 * RMzscore + r}$$

where $y_{i(age)}$ stands for the NDI value in each white matter cluster of the i^{th} subject at the age at the time of the scan and *sex* represents the sex information of the i^{th} subject. Head motion was quantified by calculating the z score of the root-mean-square (RMS) displacement of both the mean absolute (*AMzscore*) and mean relative (*RMzscore*) intervolume displacement. *r* represents the residuals, and the nonparametric term s(*age)* represents the age of the i^{th} subject.

On the basis of these fitted models, we further calculated the first derivatives to represent growth rates. The estimated nonparametric functions *s(age)* were obtained using cubic splines[46] in R version 4.2.1.

In the cubic spline function, the entire age range was divided into 100 intervals of equal size, and each interval was represented by a cubic equation. *s(age)* can be represented using the following formula:

$$s(age)=a*(x_i - x_0)\ ^3+b*\ (x_i - x_0)\ ^2+c*\ (x_i - x_0) +d$$

where x_i represents the age of the i^{th} subject, and x_0 represents the starting age of the interval to which the i^{th} subject belongs. The smoothing parameter, effective degrees of freedom (EDFs), R-squared and Akaike information criterion (AIC) were shown in Supplementary Table 3. The EDF values formed by GAM showed the degree of the curvature of the relationship.

Next, we then calculated the derivatives of these growth rates (i.e., the second derivatives of the GAM-estimated curves) to identify critical transition time points in early childhood. We used two time points to define the developmental stages: 1) time point 1, where the derivative of the growth rate reached its minimum value, indicating the period of maximal deceleration in growth; 2) time point 2, where the derivative returned to zero, marking the onset of the plateau period in early childhood. These inflection points correspond to the transitions between our fast, moderate, and slow-developing stages. Notably, for the CC Cluster, there were two special cases of defining the second special point: The first was that in the TD group, the second special time point was defined at the changing point of the derivative of the growth rate at 5 years of age, which was close to zero. The second was that in the ASD with DD/ID group, the second special time point was defined as approximately 6.07 years of age when the growth rate reached 0. Therefore, for early white matter development, we defined the fast stage as the period before time point 1, the slow stage as the period after time point 2, and the moderate stage as the period between these two special time points.

Group comparisons at various stages of early white matter development

For each white matter cluster, we performed a general linear model (GLM) in MATLAB 2020a to evaluate group differences in both the NDI value and growth rate of NDI at each stage. Specifically, we calculated the first derivative of each participant's developmental curve at their specific age. Notably, the moderate and slow developmental stages were combined as a moderate-slow stage due to their short durations. Age, sex, and head motion during the MRI scan were included as covariates to account for potential confounding effects.

Correlation analyses between the NDI of each cluster and clinical symptoms

For the ASD and DD/ID groups, we performed partial correlation analyses between the NDI of each cluster and cognitive performance and social deficits in each developmental stage and across the entire age range, with age, sex, and head motion during the MRI scan as covariates. In each group, FDR correction using Benjamini–Hochberg correction was conducted for each scale within each cluster and stage.

Validation analyses

For the cross-section dataset, the split-half and male-only subsample validations were conducted to assess spatial and temporal developmental patterns. Additionally, we validated the temporal pattern of the developmental curves in the longitudinal subdataset. Developmental curves of FA in those white matter clusters were also delineated in main dataset.

Associations between NDI and Metabolomics and proteins blood measurements

For correlation analysis, we selected participants with both imaging data and metabolite or protein profiling available. Among individuals with ASD, 28 participants had imaging and metabolite profiling data (9 without DD/ID, 19 with DD/ID), while 29 participants had both imaging and protein profiling data (9 without DD/ID, 20 with DD/ID). To maximize sample size for correlation analysis, we combined both ASD subgroups. We employed a generalized linear model to examine the associations between the mean NDI in each cluster and the metabolites and proteins, adjusting for age, sex, and head motion during MRI scans. Significant correlations were defined when *P* values were smaller than 0.01.

Results

Sample characteristics

We included 364 participants in early childhood, comprising 160 TD children (age range: 1.2-7.9 years, 49.4% males), 51 children diagnosed as ASD without DD/ID (age range: 1.7-7.9 years, 82.4% males), 105 children diagnosed as ASD with DD/ID (age range: 1.6-7.9 years, 87.6% males), and 48 children with DD/ID (age range: 2.3-7.8 years, 35.2% males). A total of 40 participants were excluded after MR image quality control (see the Supplementary Methods 1 and Supplementary Fig. 1 for details about the exclusion criteria). The demographics of the participants and the clinical measures of children were summarized in Table 1 and Supplementary Data 4.

Consistent clustering outcomes of white matter across early childhood in typical and atypical development

We first examined the sensitivity of NODDI metrics to white matter development, and observed that NDI increased rapidly with age in early childhood while ODI exhibited a plateau pattern without age effects (Supplementary Results 1 and Supplementary Fig. 2). Therefore, we used NDI (i.e., a marker of axon

density) for the following analyses.

We first revealed the distinct spatial layout of white matter development during early childhood. We grouped core white matter regions into clusters using a hybrid hierarchical clustering algorithm[44] based on the similarity of their mean NDIs. A total of 36 core white matter regions were carefully defined using the ICBM-DTI-81 white matter atlas[40] and the white matter skeleton of the study-specific group template (see Fig. 1c, Methods and Supplementary Table 1). The clustering results were consistent in all four groups in early childhood: the optimal number of clusters according to the knee plots of inter-cluster Euclidean distances was three (Fig. 2a and Supplementary Fig. 3e-g for the hierarchical dendrograms for the TD, ASD without DD/ID, ASD with DD/ID and DD/ID groups, respectively; Supplementary Fig. 3a-d for plots of the searches for the optimal cluster numbers).

These three clusters of core white matter regions were as follows: 1) Cluster 1, mainly comprising the CC (blue in Fig. 2b, referred to as the CC Cluster); 2) Cluster 2, mainly composed of anterior and superior white matter (pink in Fig. 2b, referred to as the A-S Cluster); and 3) Cluster 3, mainly composed of posterior and inferior white matter (green in Fig. 2b, referred to as the P-I Cluster) (see Supplementary Table 1 for the list of white matter regions of interest (ROIs) in each cluster).

We next delineated the developmental curves of white matter clusters using the GAM[21]. For all three white matter clusters in the typical and atypical development groups, the NDI increased with age throughout early childhood (*P* values for each cluster, TD: $<1\times10^{-15}$; ASD without DD/ID: $<1\times10^{-15}$; ASD with DD/ID: $<1\times10^{-5}$; DD/ID: <0.016) (Fig. 2c). Notably, the CC Cluster always had the highest mean NDI. The P-I Cluster was characterized by the lowest mean NDI and the flattest developmental curve. Furthermore, the A-S Cluster showed the most rapid increase in the NDI in the initial period of early childhood development.

Growth rates and developmental stages of early white matter maturation

For the white matter clusters, we next defined the growth rates of the NDI using the first derivatives of the developmental curves. We observed that all the groups except the DD/ID group exhibited a similar pattern of white matter growth, with a rapid increase at first and a gradual transition into a platform (solid line in Fig. 3). Moreover, the groups with DD/ID (ASD with DD/ID and DD/ID groups) always had lower growth rates across all white matter clusters than the groups without DD/ID (ASD without DD/ID and TD groups).

Based on the changes of growth rate (dotted line in Fig. 3), we divided the early childhood into three stages: a fast stage with a high rate, a moderate stage with a relatively low rate, and a slow stage with a low rate (shadowed areas in Fig. 3 and Fig. 4, left column). Specifically, the TD group remained in the fast developmental stage until 3.84 years of age and entered the slow stage at about 5 years of age across all white matter clusters. The two ASD subgroups had different durations of the fast stages across white matter clusters. The fast stage of the A-S Cluster and P-I Cluster stopped after 4 years of age, which was slightly longer than the fast stage of the TD group. In contrast, the fast stage of the CC cluster ended before 3 years of age in the ASD without DD/ID group. Additionally, the ASD with DD/ID group entered the slow stage after 6 years of age in the CC Cluster but had almost no slow stage in the other clusters. In contrast, the DD/ID group had no clearly defined developmental stages, as it lacked variability in the growth rate of the NDI throughout early development (see Supplementary Table 4 for the time points of the developmental stages). As the slow stage did not emerge in some scenarios, we combined the two non-fast stages—the moderate and slow stages—into one, a moderate-slow stage, for the following analysis.

During the fast stage, the growth rates of the ASD with DD/ID group were the lowest across all clusters (P values $<1\times10^{-9}$). In addition, the ASD without DD/ID group had significantly lower rates in the A-S

Cluster and P-I Cluster but a higher rate in the CC Cluster than the TD group (P values $<1\times10^{-6}$). In the moderate-slow stage, the growth rates of the A-S Cluster and P-I Cluster in both ASD subgroups were significantly higher than those in the TD group (P values <0.004, false discovery rate (FDR)-corrected P values <0.01). Across the entire age range, the ASD with DD/ID group had significantly lower growth rates in all white matter clusters than the TD and ASD without DD/ID groups (P values<0.02, FDR-corrected P values<0.05). Moreover, compared with the TD group, the ASD without DD/ID group showed a higher growth rate in the CC Cluster (P=0.019, FDR-corrected P<0.05) but a lower growth rate in the P-I Cluster (P=0.020, FDR-corrected P<0.05). In addition, the growth rates of the DD/ID group were significantly lower than those of the TD group in the P-I Cluster ($P<1\times10^{-4}$, FDR-corrected P<0.05) and lower than those of the ASD without DD/ID group in the CC Cluster and A-S Cluster (P values<0.03, FDR-corrected P values<0.05) (Fig. 4, middle column and Supplementary Table 5).

We also performed group comparisons of the mean NDI of the white matter clusters according to the developmental stages (Fig. 4, right column). The TD group showed a significantly higher NDI in the moderate-slow stage than in the fast stage in all white matter clusters (P values<0.007). Meanwhile, for the ASD without DD/ID group, the NDI in the moderate-slow stage was higher than that in the fast stage in the CC Cluster (P=0.033). At each developmental stage, there were no significant group differences in the NDI for any of the white matter clusters. Across the entire age range, the DD/ID group had a lower NDI than the TD group in the P-I Cluster (P=0.014, FDR-corrected P<0.05) and a lower NDI than the ASD with DD/ID group across all clusters (P values<0.003, FDR-corrected P values<0.05), while there was no significant difference in the NDI among the two ASD subgroups and TD group (Supplementary Tables 6 and 7).

Associations between the NDI of white matter clusters and social symptoms and cognitive

performance in ASD and DD/ID children

To evaluate the clinical relevance of the neuroimaging findings, we performed partial correlations between the mean NDI of white matter clusters and the social symptoms and cognitive performance in young children with atypical development (including the ASD without DD/ID, ASD with DD/ID and DD/ID groups). Notably, the moderate and slow developmental stages were combined into the moderate-slow stage due to their short durations (the same reason mentioned in the previous subsection). The relationships between the NDI of white matter clusters and clinical measurements of the ASD subgroups varied across developmental stages. In the fast stage, for the ASD with DD/ID group, we observed: 1) the NDI in the P-I Cluster was negatively correlated with the adaptive development quotient (DQ) (r=-0.343, P=0.006, FDR-corrected P<0.05) and average DQ (r=-0.313, P=0.012, FDR-corrected P<0.05); 2) the NDI in the A-S Cluster was negatively correlated with the fine motor DQ (r=-0.443, P=0.008, FDR-corrected P<0.05) (Fig. 5a; Supplementary Tables 8 and 9). At the moderate-slow stage, for the ASD without DD/ID group, the NDI of the CC Cluster was negatively correlated with the scores of social deficits measured by the Social Awareness subscale of the SRS[32] (r=-0.565, P=0.006, FDR-corrected P<0.05) (Fig. 5b; Supplementary Tables 10 and 11). Across the entire age range, we identified that for the ASD without DD/ID group, the NDI in the CC Cluster was negatively correlated with Autism Diagnostic Observation Schedule (ADOS)[26] restricted, repetitive behavior calibrated severity score (RRB_CSS) (r=-0.370, P=0.011, FDR-corrected P<0.05). In the DD/ID group, there was no significant correlation between the NDI and clinical measurements (Supplementary Tables 12-14). In addition, we provided a complete list of correlation results in Supplementary Tables 8-14 for completeness and transparency.

Validation analyses

A series of validation analyses were conducted to assess the robustness of our findings. First, the spatial and temporal developmental patterns were validated in the cross-section dataset, using the split-half and male-only subsamples (Supplementary Results 2, Supplementary Fig. 4 to 7). Second, the temporal developmental pattern was further validated using the subset with longitudinal data (Supplementary Fig. 8, the demographics and clinical measures of children with ASD in longitudinal subset were shown in Supplementary Table 15). In addition, as FA is widely used in diffusion MRI studies, demonstrating similar FA developmental trajectories in our dataset would indicate that our population and data quality are comparable with those in previous studies, thereby supporting the generalizability of our NDI findings derived from NODDI. Therefore, developmental trajectories of FA in the three white matter clusters were also delineated using the cross-section dataset (Supplementary Fig. 9 and 10).

Axon density of white matter clusters in ASD are linked with blood metabolic and protein profiles

For the subsample of 28 individuals with ASD with both imaging and metabolite profiling data, we found that multiple metabolites were significantly associated with the mean NDI of the A-S Cluster (Creatine, uncorrected P=0.0055; 3-Hydroxyanthranilic acid, uncorrected P=0.0019) and the P-I Cluster (Alloxan, uncorrected P=0.0069; p-Hydroxymandelic acid, uncorrected P=0.0028; Pelargonin, uncorrected P=0.0051; 3-Hydroxyanthranilic acid, uncorrected P=0.0021) respectively. However, none of metabolites was associated with NDI of the CC Cluster (Supplementary Table 16). In addition, for the subsample of 29 individuals with ASD with both imaging and protein profiling data, we identified 9 proteins were significantly associated with the mean NDI of the A-S Cluster, 9 proteins in the P-I Cluster, and 8 proteins in the CC Cluster (uncorrected P <0.05). See more details of the protein measurements and the respective statistics in Supplementary Data 5.

Discussion

Using NODDI, we investigated the spatial and temporal patterns of white matter microstructure development and their relationship with clinical traits in two ASD subgroups compared with TD and DD/ID groups in early childhood. This study yielded several primary insights. First, consistent with the TD group, the same three white matter clusters were identified among the two ASD groups and the DD/ID group, indicating that the spatial layout of white matter was conserved in children with both typical and atypical early development. Secondly, three stages with successively lower developmental rates were identified in children with ASD, which were similar to those of TD children but delayed overall with a more severe manifestation in ASD with DD/ID children. In contrast, the DD/ID group was characterized by uniform and slow rates without defined stages. Moreover, the cognitive performance of the ASD with DD/ID group were correlated with the NDI in the A-S and P-I clusters at the fast developmental stage, while the social deficits of the ASD without DD/ID group were correlated with the NDI of the CC Cluster during the moderate-slow stage. Finally, NDIs of white matter clusters were associated with multiple metabolic and protein measurements in ASD.

In this study, we observed the unique spatial layout of white matter tracts with coordinated development of axon density in early typical and atypical childhood. Although previous studies indicated spatial heterogeneities in white matter during early childhood[12,47], we revealed the coordinated pattern white matter development during early childhood, reflected by the same three white matter cluster, using NDI to the best of our knowledge. Our findings suggested that axon density was not spatially evenly distributed, and various biological mechanisms in distinct regions may underlie the spatial developmental pattern during

early childhood, including axon growth and axon alignments in white matter[48-50]. Specifically, the CC Cluster, mainly including the CC, was characterized by the highest NDI value among the three clusters over the whole age range studied. Previous studies revealed that the CC exhibited rapid growth in the first 2 years with the earliest maturation[12,51,52], which might lead to the high density of axon packing during early childhood. Moreover, the CC is the major white matter tract for interhemispheric functional communications[53]. The high demand for such communications may be a key driving factor of the high axon density in this white matter fiber bundle during early childhood. In contrast, the A-S Cluster exhibited the highest growth rates among the three clusters. White matter in the A-S Cluster is mainly intra-hemispheric and projects to the frontal, parietal and temporal cortices. Their fast growth would foster efficient and coordinated transmissions of signals across the entire brain[47] and may facilitate rapid skill acquisition, including language and social interaction skills, in the first 7 years of life[54]. In addition, the P-I Cluster exhibited the lowest NDI value and growth rates, consistent with previous findings of the late NDI maturation until adulthood in this white matter cluster[12]. Notably, the left and right fornix/stria terminalis were classified into distinct developmental clusters, whereas all other white matter tract pairs showed were assigned to the same cluster. The stria terminalis, as a core component of the limbic circuitry, is fundamentally involved in modulating memory, emotional responses, and social behaviors[55]. In line with this, prior research utilizing large-sample diffusion MRI data in young adults has demonstrated inherent lateralization in the white matter microstructure of the fornix[56,57]. Together with our findings, these results may suggest an early-emerging and fundamental feature of neural organization, wherein these limbic pathways undergo specialized hemispheric development to support complex cognitive and social-affective functions. Furthermore, the consistency of spatial developmental patterns across all four groups indicated

that the spatial patterns of white matter axon density were unaffected by ASD or DD/ID during early childhood. In neurodevelopment, as the proto-map of the cytoarchitectonic areas is provided by the proliferative units in the cerebral ventricle[58], the spatial patterns of both neurons and axons in the brain may already be finalized before the neurophysiologies of ASD emerge[59] and remain unaffected by the expression of ASD genes afterwards. However, these questions have yet to be answered, and future studies that mimic the cellular development of the brain using organoids may be beneficial to elucidate the mechanism behind this phenomenon.

Another important finding in this study was the distinct developmental stages defined by changes in growth rates during early childhood. We detected the fast stage before 2.7 years of age with the fastest growth rates in the TD group, indicating rapid axon development before this time point. This is in line with postmortem and *in vivo* MR imaging findings that suggested a rapid increase in axon packing across the first 2-3 years of life[49,50]. The growth rates slowed during the ages of 4 to 5 years, and the axon development in the CC Cluster almost approached maturation after the age of 5 years. These observed differences in developmental trajectories and stages are likely driven by underlying biological mechanisms. Previous research has highlighted that white matter maturation involves processes such as myelination and the coordinated development between white matter tracts and cortical geometry[60]. We speculate that the differential developmental rates across clusters may be linked to heterogeneous timelines of myelination or variations in activity-dependent plasticity across specific white matter pathways. For instance, the slower developmental rate observed in one cluster might reflect prolonged sensitive periods for plasticity in certain association fibers, whereas rapid, early maturation in another could be linked to the swift myelination of primary projection tracts. Although currently hypothetical, this perspective is supported by studies showing

that structural-functional coupling in white matter continues to develop throughout adolescence and is linked to improvements in executive function[61,62]. Additionally, the stability of these clusters across populations suggests that they may represent innate patterns of white matter organization, potentially governed by genetic factors that guide the overall layout of white matter architecture, as evidenced by research on the heritability of tract-cortical geometry coupling[60]. Compared to the TD group, both ASD subgroups exhibited developmental delays with reduced growth rates. Specifically, the ASD with DD/ID group showed more severe delays than the ASD without DD/ID group, possibly due to the genetic abnormalities that result in a comprehensive alteration in axonal development in individuals with DD/ID[63,64]. Additionally, both ASD subgroups exhibited atypical increases during the fast developmental stage, indicating overgrowth of the brain during early life in individuals with ASD[65]. Interestingly, we found that of all three clusters, the ODI, a marker of the coherence of axon alignment derived from NODDI, was within the normal range in the groups with both typical and atypical neurodevelopment and showed no significant intergroup differences or age effects during early development, consistent with previous findings that the ODI was not significantly associated with age in most white matter tracts in TD[12-14]. This finding suggested that in NDDs such as ASD and DD/ID, the atypicality of core white matter during early development are associated with axon density but not the dispersion of axon alignment.

Finally, our findings unveiled the potential neurophysiological mechanisms underlying the temporal development of symptoms in children with ASD. Our findings highlighted the importance of early childhood in ASD by revealing that symptoms of cognitive and social capabilities in children with ASD were related to axon density in white matter clusters at different developmental stages. For ASD, its fast white matter axon density development was linked to cognitive outcomes, while slower and more prolonged

development was related to core behavioral features. In contrast, children with DD/ID alone lacked these distinct stages, suggesting a broader alteration in white matter development. Specifically, in the fast stage, atypical axon density growth in the A-S and P-I clusters was associated with poorer cognitive performances in the ASD with DD/ID group, especially for the fine motor DQ and adaptive DQ. This could be attributed to the associations of white matter in these two clusters with general cognitive performance, especially executive function and visual-motor performance, which would have an impact on the fine motor DQ and adaptive DQ[66,67]. In the later moderate-slow stages, axon density growth of the CC cluster was associated with milder social deficits in the ASD without DD/ID group. This further supported the importance of white matter in CC cluster in social deficits of ASD children[4,52,68]. These findings help delineate critical neurodevelopmental windows during which specific cognitive and behavioral profiles emerge. They provide a potential imaging-based framework for stratifying the heterogeneous ASD population—for example, by distinguishing individuals with primarily cognitive developmental trajectories from those with predominantly behavioral developmental pathways, or by identifying a DD/ID child with globally altered white matter growth. Our results align conceptually with a recent study published in Nature[69] that reported distinct developmental trajectories between early- and late-diagnosed autistic individuals. This convergence of evidence underscores the importance of timing and phase-specific brain maturation in understanding ASD heterogeneity. Our findings extend this concept by revealing that different developmental phases are preferentially associated with either cognitive or behavioral dimensions of the condition.

Besides, previous studies have reported sex differences in white matter structure among early-stage children with ASD. Some evidence suggests that ASD girls exhibit broader or more pronounced white matter alterations compared to boys, including enlargement of temporal gray and white matter volumes and

reduced cerebellar gray matter and corpus callosum fibers[70]. Similarly, ASD girls aged 3–5 years have shown more widespread cortical differences involving multiple functional networks[71]. However, studies in infants around 6–7 months have found no significant sex differences in white matter microstructure[72], suggesting that such differences may emerge within specific developmental windows. Longitudinal analyses of children aged 3–5 years have also reported no diagnostic or sex effects on the rate of change in corpus callosum diffusion measures[73]. In contrast, other research indicates that autistic females may undergo faster cortical thinning over time[71]. Together, these findings suggest that sex-related differences in early white matter development in ASD may be dynamic, potentially reflecting distinct temporal trajectories across early growth stages. Developmental patterns in our study were primarily characterized by ASD boys. However, due to the limited sample size of female participants, we were unable to further explore sex-specific patterns which were supposed to clarify in our future studies.

The altered development of axon density in ASD children appears to have both metabolic and protein associations. In terms of metabolomics, 3-Hydroxyanthranilic Acid, known for its neuroactive properties, can influence neuroinflammation and neurotoxicity[74]. Dysregulation in this pathway can affect neuronal health and potentially affect axon density. Alloxan is known to induce oxidative stress and mitochondrial dysfunction – pathways implicated in ASD pathophysiology. Its presence in the metabolic profile suggests a potential role for reactive oxygen species (ROS)-mediated mechanisms in a subgroup of individuals with ASD, which aligns with growing evidence of redox imbalance in the disorder. The direct impact of p-Hydroxymandelic Acid on neurite density and neural development in ASD remains unclear. For the protein - Caspase 9 (CASP9), a key component of the intrinsic apoptosis pathway, is crucial for programmed cell death. Its activation can lead to axonal degeneration and neuronal death, both critical to neurodevelopment

and neurodegeneration[75]. Another protein - Enolase 1 (ENO1), also known as neuron-specific enolase (NSE), serves as a marker for neuronal cells and its levels were elevated in children with ASD[76,77]. ENO1 is increasingly recognized for its neurotrophic functions and has been identified as an autoantigen in other neurological conditions. Its altered expression in our proteomic data may indicate disruptions in neuronal survival or synaptic maintenance pathways. While several other proteins are indicated to be potentially correlated with neurodevelopment, their precise relationships with axon development in ASD children remain unclear. Future studies are needed to clarify the mechanisms by which these metabolites and proteins influence neurodevelopment and to explore their potential as clinical therapeutic targets in ASD.

Several limitations in the current study should be stated. First, though no children with ASD or DD/ID with any medication history before the MRI scan were included, some had already received behavioral interventions, especially older children, which might partly have an impact on the estimation of their representative developmental curves. Second, the effect of sex is an important factor in ASD research. Although we observed consistent findings in the male-only subsample for validation, including more female participants in future studies would be helpful to reveal sex differences in the developmental patterns of children with ASD. Third, though our use of full k-space acquisition effectively avoided bed-vibration artefacts[78], it requires relatively long scan time. As shorter acquisition time could greatly improve the success rate of MR scans in young populations, we recommend placing heavy sandbags on the scanner bed - as implemented in Baby Connectome Project[79] - to stabilize the bed and enable the use of shorter partial-Fourier acquisitions. Fourthly, though NODDI metrics have been validated histologically[11] and are now widely adopted for microstructure imaging of the brain, it is important to recognize that NODDI models has several limitations – for example, the assumption of fixed intrinsic diffusivity[80]. Fifthly, long-term

longitudinal neuropsychological assessments would further strengthen the significance of our findings, and such follow-up visits will be incorporated in the future phase of our project. Sixthly, most of metabolomic and proteomic analyses did not survive FDR correction, maybe due to the small sample size with the large number of measured variables. Besides, although we conducted validations using split-half and male-only subsamples, we still lacked an external dataset suitable for independent validation. Future studies with larger sample sizes and external validation cohorts would strengthen these findings. Seventhly, cognitive assessments used different scales before and after age 4, potentially compromising age-related continuity and comparability of cognitive measures between development stages. Finally, although longitudinal subdataset had limited sample sizes due to the challenges of collecting imaging data from children in the early childhood, we observed the similar manifestations on developmental curves in longitudinal analysis. Future longitudinal studies with a larger sample size would be beneficial to further elucidate the patterns of white matter development in this critical period of life.

In conclusion, we identified similar coordinated development pattern of white matter in ASD, with or without DD/ID, as typical development, evidenced by the same three white matter clusters, but with altered developmental trajectories. Moreover, NDI of these white matter clusters in ASD was: a) correlated with cognitive impairments at the stage with a fast developmental pace and social deficits at the stage with a moderate-slow developmental pace; b) linked with multiple metabolic and protein measurements.

Acknowledgements

We thanked Dr. Yong He from Beijing Normal University and Dr. Daniel Alexander from University College London for their helpful comments and discussions. This study was supported by grants from the National Natural Science Foundation of China (82125032, 81930095, 81901826, 81761128035, 82202243,

82204048 and 82001771), the Science and Technology Commission of Shanghai Municipality (19410713500 and 2018SHZDZX01), the Shanghai Municipal Commission of Health and Family Planning (GWV-10.1-XK07, 2020CXJQ01, 2018YJRC03, 20214Y0125), the Shanghai Clinical Key Subject Construction Project (shslczdzk02902), the Shanghai Municipal Science and Technology Major Project [No.2018SHZDZX01], Innovative research team of high-level local universities in Shanghai (SHSMU-ZDCX20211100), the Guangdong Key Project (2018B030335001).

Author contributions

F.L., M.C. and J.Z. designed the study. Y.L., Y.D., S.G., L.D., Z.C., Y.Z., Y.S.,W.Z., L.Z., T.R. contributed to the acquisition of research data. Y.L., J.Z. and M.C. conducted the data analysis. F.L., M.C., J.Z. and Y.L. provided the interpretation of results. Y.L., J.Z. and M.C. wrote the first draft of the manuscript. E.T.R. and J.F. revised the manuscript.

Competing interests

The authors have no competing interests.

Data Availability Statement

The source data for Figures 2-5 is in Supplementary Data 1.

Access to the deidentified MR image data must be approved by the research ethics board on a case-by-case basis, please contact the corresponding authors (feili@shsmu.edu.cn, mcao@fudan.edu.cn, jiaying.zhang@bupt.edu.cn) for assistance in data access request.

References

1 American Psychiatric Association, DSM-5 Task Force. (2013). Diagnostic and statistical manual of mental disorders: DSM-5™ (5th ed.). American Psychiatric Publishing, Inc.. https://doi.org/10.1176/appi.books.9780890425596.

2 Hirota, T. & King, B. H. Autism Spectrum Disorder. *Jama* **329**, doi:10.1001/jama.2022.23661 (2023).

3 Wegiel, J. *et al.* Deficit of corpus callosum axons, reduced axon diameter and decreased area are markers of abnormal development of interhemispheric connections in autistic subjects. *Acta Neuropathol Commun* **6**, 143, doi:10.1186/s40478-018-0645-7 (2018).

4 Andrews, D. S. *et al.* A Longitudinal Study of White Matter Development in Relation to Changes in Autism Severity Across Early Childhood. *Biol Psychiatry* **89**, 424-432, doi:10.1016/j.biopsych.2020.10.013 (2021).

5 Ouyang, M. *et al.* Atypical age-dependent effects of autism on white matter microstructure in children of 2-7 years. *Hum Brain Mapp* **37**, 819-832, doi:10.1002/hbm.23073 (2016).

6 Solso, S. *et al.* Diffusion Tensor Imaging Provides Evidence of Possible Axonal Overconnectivity in Frontal Lobes in Autism Spectrum Disorder Toddlers. *Biol Psychiatry* **79**, 676-684, doi:10.1016/j.biopsych.2015.06.029 (2016).

7 Wolff, J. J. *et al.* Differences in white matter fiber tract development present from 6 to 24 months in infants with autism. *Am J Psychiatry* **169**, 589-600, doi:10.1176/appi.ajp.2011.11091447 (2012).

8 Jones, D. K., Knösche, T. R. & Turner, R. White matter integrity, fiber count, and other fallacies: the do's and don'ts of diffusion MRI. *Neuroimage* **73**, 239-254, doi:10.1016/j.neuroimage.2012.06.081 (2013).

9 Beaulieu, C. The basis of anisotropic water diffusion in the nervous system - a technical review. *NMR Biomed* **15**, 435-455, doi:10.1002/nbm.782 (2002).

10 Zhang, H., Schneider, T., Wheeler-Kingshott, C. A. & Alexander, D. C. NODDI: practical in vivo neurite orientation dispersion and density imaging of the human brain. *Neuroimage* **61**, 1000-1016, doi:10.1016/j.neuroimage.2012.03.072 (2012).

11 Grussu, F. *et al.* Neurite dispersion: a new marker of multiple sclerosis spinal cord pathology? *Ann Clin Transl Neurol* **4**, 663-679, doi:10.1002/acn3.445 (2017).

12 Lynch, K. M., Cabeen, R. P., Toga, A. W. & Clark, K. A. Magnitude and timing of major white matter tract maturation from infancy through adolescence with NODDI. *Neuroimage* **212**, 116672, doi:10.1016/j.neuroimage.2020.116672 (2020).

13 Dimond, D. *et al.* Maturation and interhemispheric asymmetry in neurite density and orientation dispersion in early childhood. *Neuroimage* **221**, 117168, doi:10.1016/j.neuroimage.2020.117168 (2020).

14 Zhao, X. *et al.* Brain Development From Newborn to Adolescence: Evaluation by Neurite Orientation Dispersion and Density Imaging. *Front Hum Neurosci* **15**, 616132, doi:10.3389/fnhum.2021.616132 (2021).

15 Yasuno, F. *et al.* Microstructural Anomalies Evaluated by Neurite Orientation Dispersion and Density Imaging Are Related to Deficits in Facial Emotional Recognition via Perceptual-Binding Difficulties in Autism Spectrum Disorder. *Autism Res* **13**, 729-740, doi:10.1002/aur.2280 (2020).

16 Matsuoka, K. *et al.* Increased Dendritic Orientation Dispersion in the Left Occipital Gyrus is Associated

with Atypical Visual Processing in Adults with Autism Spectrum Disorder. *Cereb Cortex* **30**, 5617-5625, doi:10.1093/cercor/bhaa121 (2020).

17 Kitamura, S. *et al.* Association of adverse childhood experience-related increase in neurite density with sensory over-responsivity in autism spectrum disorder: A neurite orientation dispersion and density imaging study. *J Psychiatr Res* **161**, 316-323, doi:10.1016/j.jpsychires.2023.03.029 (2023).

18 Andica, C. *et al.* Neurite orientation dispersion and density imaging reveals white matter microstructural alterations in adults with autism. *Mol Autism* **12**, 48, doi:10.1186/s13229-021-00456-4 (2021).

19 Dean, D. C., 3rd *et al.* Multivariate characterization of white matter heterogeneity in autism spectrum disorder. *Neuroimage Clin* **14**, 54-66, doi:10.1016/j.nicl.2017.01.002 (2017).

20 Yoon, C. D. & Dean, D. C., 3rd. Advanced Quantitative Microstructure Imaging in Autism: A Review of Methodology, Group Differences, and Associations With Developmental Outcomes. *Autism Res* **18**, 2140-2165, doi:10.1002/aur.70122 (2025).

21 Hastie, T.J. (1990). Generalized Additive Models (1st ed.). Routledge. https://doi.org/10.1201/9780203753781.

22 Al Rasbi, Z. *et al.* The role of interleukin-37 and interleukin-38 in the development and remission of autism spectrum disorder: a comprehensive review of neuroinflammatory mechanisms and potential therapeutic implications. *Front Immunol* **16**, 1716197, doi:10.3389/fimmu.2025.1716197 (2025).

23 Nautiyal, H., Roy, K. K. & Dwivedi, S. BDNF- Dysregulation as a Neurobiological Bridge between Polycystic Ovarian Syndrome and Autism Spectrum Disorder. *ACS Chem Neurosci* **17**, 870-885, doi:10.1021/acschemneuro.5c00574 (2026).

24 Dhungel, A. & Bora, R. Unraveling mGluR5 dysfunction in autism spectrum disorder: a multi-level analysis of genetic, molecular, and neurobiological mechanisms. *J Neural Transm (Vienna)*, doi:10.1007/s00702-026-03116-0 (2026).

25 Dai, Y. *et al.* Shanghai Autism Early Development: An Integrative Chinese ASD Cohort. *Neurosci Bull* **38**, 1603-1607, doi:10.1007/s12264-022-00904-y (2022).

26 Lord, C. *et al.* The autism diagnostic observation schedule-generic: a standard measure of social and communication deficits associated with the spectrum of autism. *J Autism Dev Disord* **30**, 205-223 (2000).

27 Hus, V., Gotham, K. & Lord, C. Standardizing ADOS domain scores: separating severity of social affect and restricted and repetitive behaviors. *J Autism Dev Disord* **44**, 2400-2412, doi:10.1007/s10803-012-1719-1 (2014).

28 Wang, Y. *et al.* Prenatal and postnatal exposure to organophosphate pesticides and childhood neurodevelopment in Shandong, China. *Environ Int* **108**, 119-126, doi:10.1016/j.envint.2017.08.010 (2017).

29 Wechsler, D. (2002). Wechsler preschool and primary scale of intelligence (3rd ed.). San Antonio, TX: Psychological Corporation.

30 Wechsler, D. (2003). Wechsler intelligence scale for children (4th ed.). San Antonio: The Psychological Corporation.

31 Moon, S. J. *et al.* Accuracy of the Childhood Autism Rating Scale: a systematic review and meta-analysis. *Dev Med Child Neurol* **61**, 1030-1038, doi:10.1111/dmcn.14246 (2019).

32 Bölte, S., Poustka, F. & Constantino, J. N. Assessing autistic traits: cross-cultural validation of the social responsiveness scale (SRS). *Autism Res* **1**, 354-363, doi:10.1002/aur.49 (2008).

33 Geng, H. *et al.* The dosimetric effect of zipper artifacts on tomotherapy adaptive dose calculation--a phantom study. *Med Dosim* **36**, 306-312, doi:10.1016/j.meddos.2010.06.002 (2011).

34 Tournier, J. D. *et al.* MRtrix3: A fast, flexible and open software framework for medical image processing and visualisation. *Neuroimage* **202**, 116137, doi:10.1016/j.neuroimage.2019.116137 (2019).

35 Smith, S. M. *et al.* Advances in functional and structural MR image analysis and implementation as FSL. *Neuroimage* **23 Suppl 1**, S208-219, doi:10.1016/j.neuroimage.2004.07.051 (2004).

36 Cordero-Grande, L., Christiaens, D., Hutter, J., Price, A. N. & Hajnal, J. V. Complex diffusion-weighted image estimation via matrix recovery under general noise models. *Neuroimage* **200**, 391-404, doi:10.1016/j.neuroimage.2019.06.039 (2019).

37 Kellner, E., Dhital, B., Kiselev, V. G. & Reisert, M. Gibbs-ringing artifact removal based on local subvoxel-shifts. *Magn Reson Med* **76**, 1574-1581, doi:10.1002/mrm.26054 (2016).

38 Graham, M. S., Drobnjak, I., Jenkinson, M. & Zhang, H. Quantitative assessment of the susceptibility artefact and its interaction with motion in diffusion MRI. *PLoS One* **12**, e0185647, doi:10.1371/journal.pone.0185647 (2017).

39 Tustison, N. J. *et al.* N4ITK: improved N3 bias correction. *IEEE Trans Med Imaging* **29**, 1310-1320, doi:10.1109/tmi.2010.2046908 (2010).

40 Mori, S. *et al.* Stereotaxic white matter atlas based on diffusion tensor imaging in an ICBM template. *Neuroimage* **40**, 570-582, doi:10.1016/j.neuroimage.2007.12.035 (2008).

41 Modat, M. *et al.* Fast free-form deformation using graphics processing units. *Comput Methods Programs Biomed* **98**, 278-284, doi:10.1016/j.cmpb.2009.09.002 (2010).

42 Zhang, H., Yushkevich, P. A., Alexander, D. C. & Gee, J. C. Deformable registration of diffusion tensor MR images with explicit orientation optimization. *Med Image Anal* **10**, 764-785, doi:10.1016/j.media.2006.06.004 (2006).

43 Yuan, M., Breitkopf, S. B., Yang, X. & Asara, J. M. A positive/negative ion-switching, targeted mass spectrometry-based metabolomics platform for bodily fluids, cells, and fresh and fixed tissue. *Nat Protoc* **7**, 872-881, doi:10.1038/nprot.2012.024 (2012).

44 Chipman, H. & Tibshirani, R. Hybrid hierarchical clustering with applications to microarray data. *Biostatistics* **7**, 286-301, doi:10.1093/biostatistics/kxj007 (2006).

45 Bethlehem, R. A. I. *et al.* Brain charts for the human lifespan. *Nature* **604**, 525-533, doi:10.1038/s41586-022-04554-y (2022).

46 Ruppert, D., Wand, M. P. & Carroll, R. J. Semiparametric regression during 2003-2007. *Electron J Stat* **3**, 1193-1256, doi:10.1214/09-ejs525 (2009).

47 Grotheer, M. *et al.* White matter myelination during early infancy is linked to spatial gradients and myelin content at birth. *Nat Commun* **13**, 997, doi:10.1038/s41467-022-28326-4 (2022).

48 Paus, T. Tracking Development of Connectivity in the Human Brain: Axons and Dendrites. *Biol Psychiatry* **93**, 455-463, doi:10.1016/j.biopsych.2022.08.019 (2023).

49 Lebel, C. & Deoni, S. The development of brain white matter microstructure. *Neuroimage* **182**, 207-218, doi:10.1016/j.neuroimage.2017.12.097 (2018).

50 Miller, D. J. *et al.* Prolonged myelination in human neocortical evolution. *Proc Natl Acad Sci U S A* **109**,

16480-16485, doi:10.1073/pnas.1117943109 (2012).

51 Gilmore, J. H., Knickmeyer, R. C. & Gao, W. Imaging structural and functional brain development in early childhood. *Nat Rev Neurosci* **19**, 123-137, doi:10.1038/nrn.2018.1 (2018).

52 Wolff, J. J. *et al.* Altered corpus callosum morphology associated with autism over the first 2 years of life. *Brain* **138**, 2046-2058, doi:10.1093/brain/awv118 (2015).

53 Aboitiz, F. & Montiel, J. One hundred million years of interhemispheric communication: the history of the corpus callosum. *Braz J Med Biol Res* **36**, 409-420, doi:10.1590/s0100-879x2003000400002 (2003).

54 Geng, F., Botdorf, M. & Riggins, T. How Behavior Shapes the Brain and the Brain Shapes Behavior: Insights from Memory Development. *J Neurosci* **41**, 981-990, doi:10.1523/jneurosci.2611-19.2020 (2021).

55 Kamali, A., Hosseini, M., Gandhi, A., Lincoln, J. A. & Hasan, K. M. Unfolding the direct connectivity of the occipital cortex with the hypothalamic, septal and BNST nuclei of the human brain. *Brain Res* **1817**, 148510, doi:10.1016/j.brainres.2023.148510 (2023).

56 Tsuchida, A. *et al.* Age-Related Variations in Regional White Matter Volumetry and Microstructure During the Post-adolescence Period: A Cross-Sectional Study of a Cohort of 1,713 University Students. *Front Syst Neurosci* **15**, 692152, doi:10.3389/fnsys.2021.692152 (2021).

57 Sousa, É. *et al.* Stria Terminalis: An intraoperative image. *Brain Spine* **4**, 104144, doi:10.1016/j.bas.2024.104144 (2024).

58 Rakic, P. Specification of cerebral cortical areas. *Science* **241**, 170-176, doi:10.1126/science.3291116 (1988).

59 Hutsler, J. J. & Casanova, M. F. Review: Cortical construction in autism spectrum disorder: columns, connectivity and the subplate. *Neuropathol Appl Neurobiol* **42**, 115-134, doi:10.1111/nan.12227 (2016).

60 Li, D. *et al.* Mapping the coupling between tract reachability and cortical geometry of the human brain. *Nat Commun* **16**, 7489, doi:10.1038/s41467-025-62812-9 (2025).

61 Bagautdinova, J. *et al.* Development of white matter fiber covariance networks supports executive function in youth. *Cell Rep* **42**, 113487, doi:10.1016/j.celrep.2023.113487 (2023).

62 Baum, G. L. *et al.* Development of structure-function coupling in human brain networks during youth. *Proc Natl Acad Sci U S A* **117**, 771-778, doi:10.1073/pnas.1912034117 (2020).

63 Lee, S. *et al.* Gene networks associated with non-syndromic intellectual disability. *J Neurogenet* **32**, 6-14, doi:10.1080/01677063.2017.1404058 (2018).

64 Cordovado, A. *et al.* SEMA6B variants cause intellectual disability and alter dendritic spine density and axon guidance. *Hum Mol Genet* **31**, 3325-3340, doi:10.1093/hmg/ddac114 (2022).

65 Courchesne, E. *et al.* The ASD Living Biology: from cell proliferation to clinical phenotype. *Mol Psychiatry* **24**, 88-107, doi:10.1038/s41380-018-0056-y (2019).

66 Lee Masson, H., Wallraven, C. & Petit, L. "Can touch this": Cross-modal shape categorization performance is associated with microstructural characteristics of white matter association pathways. *Hum Brain Mapp* **38**, 842-854, doi:10.1002/hbm.23422 (2017).

67 Hyde, C., Sciberras, E., Efron, D., Fuelscher, I. & Silk, T. Reduced fine motor competence in children with ADHD is associated with atypical microstructural organization within the superior longitudinal fasciculus. *Brain Imaging Behav* **15**, 727-737, doi:10.1007/s11682-020-00280-z (2021).

68 Vogan, V. M. *et al.* Widespread White Matter Differences in Children and Adolescents with Autism Spectrum Disorder. *J Autism Dev Disord* **46**, 2138-2147, doi:10.1007/s10803-016-2744-2 (2016).

69 Zhang, X. *et al.* Polygenic and developmental profiles of autism differ by age at diagnosis. *Nature* **646**, 1146-1155, doi:10.1038/s41586-025-09542-6 (2025).

70 Chen, C. & Van Horn, J. D. Developmental neurogenetics and multimodal neuroimaging of sex differences in autism. *Brain Imaging Behav* **11**, 38-61, doi:10.1007/s11682-015-9504-3 (2017).

71 Andrews, D. S. *et al.* Sex differences in trajectories of cortical development in autistic children from 2-13 years of age. *Mol Psychiatry* **29**, 3440-3451, doi:10.1038/s41380-024-02592-8 (2024).

72 Elison, J. T. *et al.* White matter microstructure and atypical visual orienting in 7-month-olds at risk for autism. *Am J Psychiatry* **170**, 899-908, doi:10.1176/appi.ajp.2012.12091150 (2013).

73 Nordahl, C. W. *et al.* Sex differences in the corpus callosum in preschool-aged children with autism spectrum disorder. *Mol Autism* **6**, 26, doi:10.1186/s13229-015-0005-4 (2015).

74 Zhuravlev, A. V., Zakharov, G. A., Shchegolev, B. F. & Savvateeva-Popova, E. V. Antioxidant Properties of Kynurenines: Density Functional Theory Calculations. *PLoS Comput Biol* **12**, e1005213, doi:10.1371/journal.pcbi.1005213 (2016).

75 Hyman, B. T. & Yuan, J. Apoptotic and non-apoptotic roles of caspases in neuronal physiology and pathophysiology. *Nat Rev Neurosci* **13**, 395-406, doi:10.1038/nrn3228 (2012).

76 Ramirez-Celis, A., Edmiston, E., Schauer, J., Vu, T. & Van de Water, J. Peptides of neuron specific enolase as potential ASD biomarkers: From discovery to epitope mapping. *Brain Behav Immun* **84**, 200-208, doi:10.1016/j.bbi.2019.12.002 (2020).

77 Stancioiu, F., Bogdan, R. & Dumitrescu, R. Neuron-Specific Enolase (NSE) as a Biomarker for Autistic Spectrum Disease (ASD). *Life (Basel)* **13**, doi:10.3390/life13081736 (2023).

78 Gallichan, D. *et al.* Addressing a systematic vibration artifact in diffusion-weighted MRI. *Hum Brain Mapp* **31**, 193-202, doi:10.1002/hbm.20856 (2010).

79 Howell, B. R. *et al.* The UNC/UMN Baby Connectome Project (BCP): An overview of the study design and protocol development. *Neuroimage* **185**, 891-905, doi:10.1016/j.neuroimage.2018.03.049 (2019).

80 Kamiya, K., Hori, M. & Aoki, S. NODDI in clinical research. *J Neurosci Methods* **346**, 108908, doi:10.1016/j.jneumeth.2020.108908 (2020).

Table 1. Demographic Characteristics of the Cross-sectional Dataset in this study

	ASD with DD/ID (A)	ASD without DD/ID (B)	DD/ID (C)	TD (D)	Post hoc[a]
Number	105	51	48	160	n.a.
Age, (years, mean ± sd)	3.93±1.51	4.32±1.95	5.24±1.73	4.39±1.90	C>A,*p*=0.002 C>D,*p*=0.02
Sex, (M/F)	92/13	42/9	37/11	79/81	A>D,*p*=0.00041 B>D,*p*=2.7e-09 C>D,*p*=0.008
Absolute RMS, (mm, mean ± sd)	0.43±0.15	0.45±0.23	0.45±0.28	0.56±0.63	n.s
Relative RMS, (mm, mean ± sd)	0.10±0.03	0.10±0.02	0.10±0.03	0.11±0.05	n.s

ASD, autism spectrum disorder. DD/ID, developmental delay/intellectual disability. TD, typical developing. M/F, Male/Female. Absolute RMS, root-mean-square displacement of the mean absolute intervolume displacement. Relative RMS, root-mean-square displacement of the mean relative intervolume displacement. [a] Tukey's honest significant difference criterion, $p<0.05$. n.a., not applicable. n.s., not significant.

Fig. 1 Flow diagram for the study of spatial and temporal patterns of white matter microstructure development in the ASD subgroups and DD/ID and TD groups. a-b, diffusion-weighted MR images, behavior measurements and blood sample were acquired from 364 children aged under 8 years old, including 156 children diagnosed with ASD (105 with DD/ID and 51 without DD/ID), 48 children diagnosed with only DD/ID, and 160 TD children. **c**, one group-specific tensor template and seven age-specific tensor templates were created for registration. In addition, DTI and NODDI were applied to compute FA and NDI maps, respectively. **d**, a hybrid hierarchical clustering algorithm was employed to delineate the spatial developmental patterns. **e**, temporal patterns of white matter microstructure development were characterized by growth curves, rates and developmental stages. Developmental curves were fitted for each cluster and each group. **f**, distinct associations between white matter microstructure and clinical manifestations (behaviors - cognitive performance and social symptoms, metabolic and protein measurements) in atypical development during the distinct stages and across the entire age range. DQ, developmental quotient. IQ, intelligence quotient. ADOS, Autism Diagnostic Observation Schedule. SRS, Social Responsiveness Scale. CARS, Childhood Autism Rating Scale.

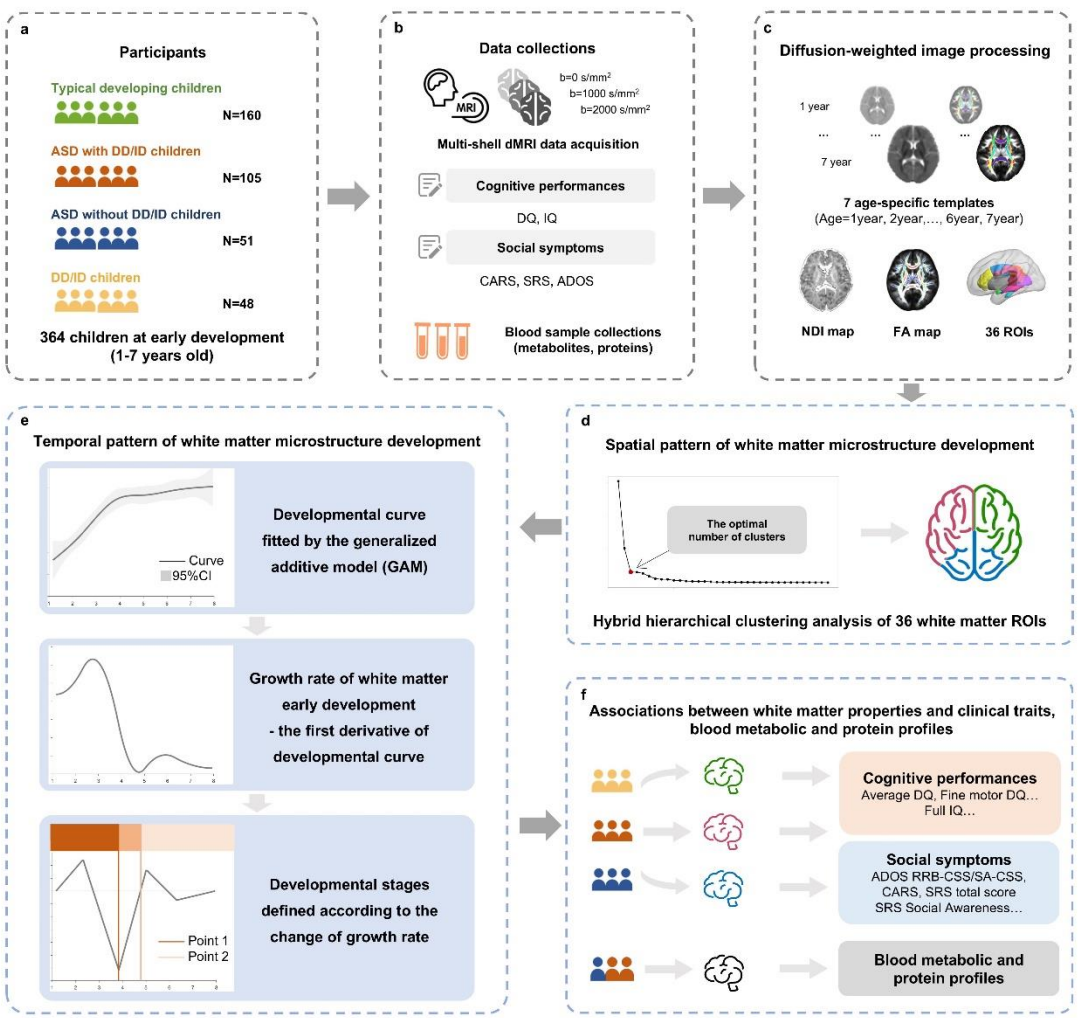

Fig. 2 Consistent clustering outcomes of white matter regions across early childhood in children with typical and atypical development. a, hybrid hierarchical dendrogram in the TD group. A total of 36 cerebral white matter regions were grouped into three clusters based on the similarity of the NDI. The CC Cluster was composed of the corpus callosum (CC), anterior limb of internal capsule (ALIC) and posterior limb of internal capsule (PLIC). The anterior-superior Cluster (A-S Cluster) was composed of the anterior corona radiata (ACR), superior corona radiata (SCR), retrolenticular internal capsule (RLIC), superior longitudinal fasciculus (SLF), superior fronto-occipital fasciculus (SFOF), left fornix (cres)/stria terminalis (FX/ST-L), fornix (FX), and cingulum bundle (CGC). The P-I Cluster was composed of the posterior corona radiata (PCR), posterior thalamic radiation (PTR), sagittal stratum (SS), external capsule (EC), right fornix (cres)/stria terminalis (FX/ST-R), uncinate fasciculus (UNC), cingulum bundle (CGH), and tapetum of commissural tracts. **b**, the spatial distribution of the white matter regions of the three clusters. **c**, developmental curves of the NDI were fitted for each cluster and each group.

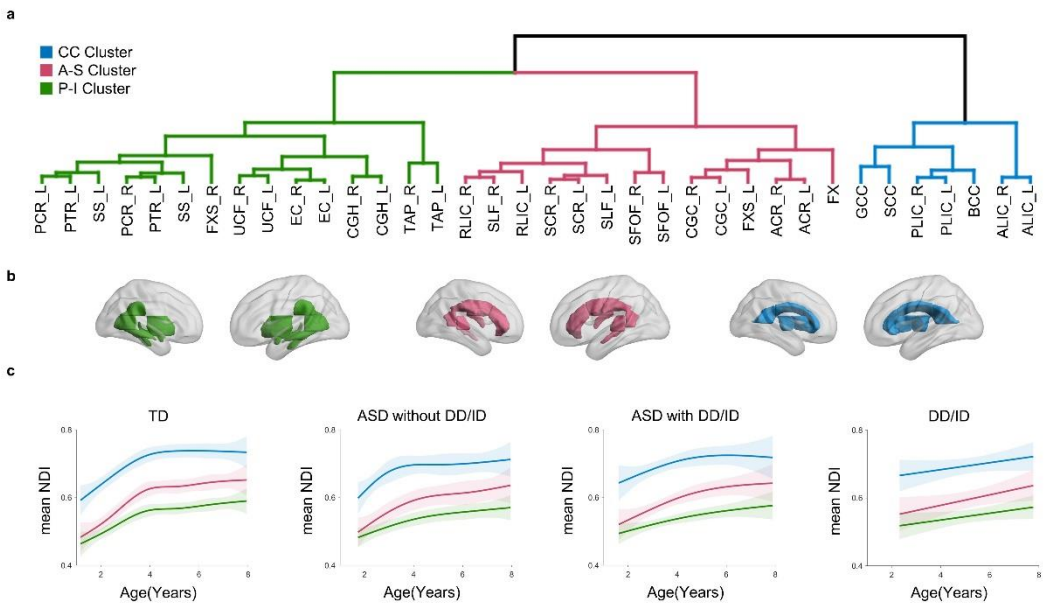

Fig. 3 Developmental curves of white matter clusters in early childhood. The growth rates of the NDI were calculated using the first derivatives of developmental curves (solid lines) and changes in rates were represented by the derivatives of the growth rates (dotted lines). Based on the changes in rates for all clusters, three developmental stages were defined using two special timepoints: the fast, moderate and slow stages (represented by dark, grey and white colors), except for DD/ID group. Growth rates and developmental stages of the TD (column 1), ASD without DD/ID (column 2), ASD with DD/ID (column 3), and DD/ID (column 4) groups.

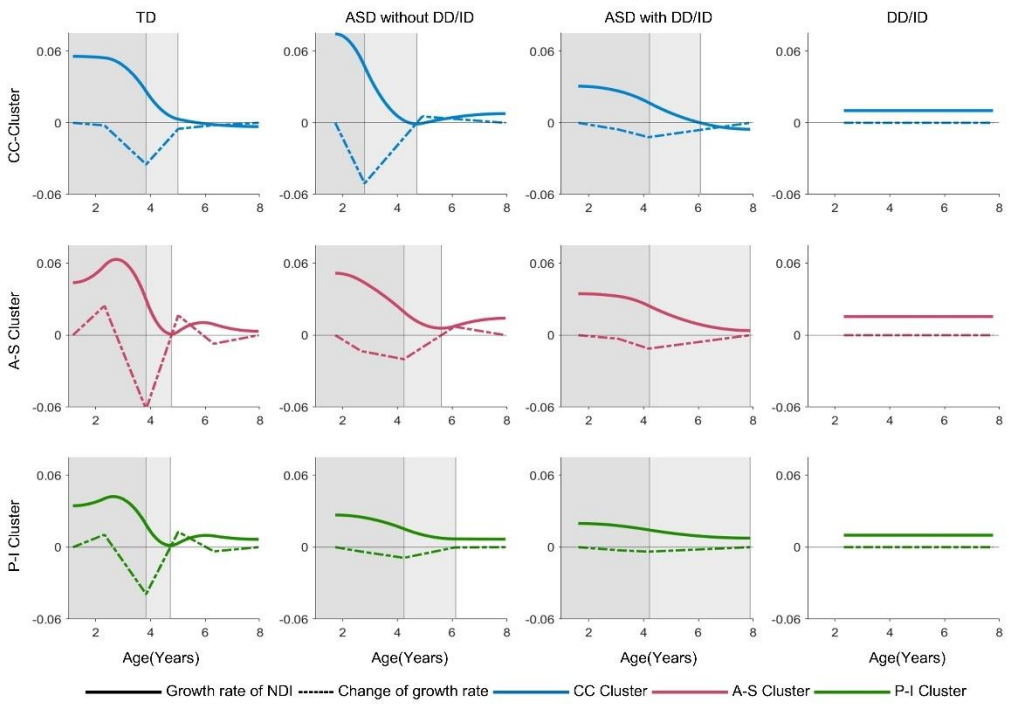

Fig. 4 Growth rates and developmental stages of early white matter development. a-c, developmental stages and box plots of the group-comparison within the CC Cluster, A-S Cluster and P-I Cluster, respectively. **Left column,** developmental stages and timepoints of each stage across all groups and all clusters. **Middle and right columns**, box plots of group comparisons of the growth rates and NDI values in each stage and across the entire age range in the CC Cluster (row 1), A-S Cluster (row 2) and P-I Cluster (row 3). The moderate and slow stages were combined into the moderate-slow stage for statistical analyses.

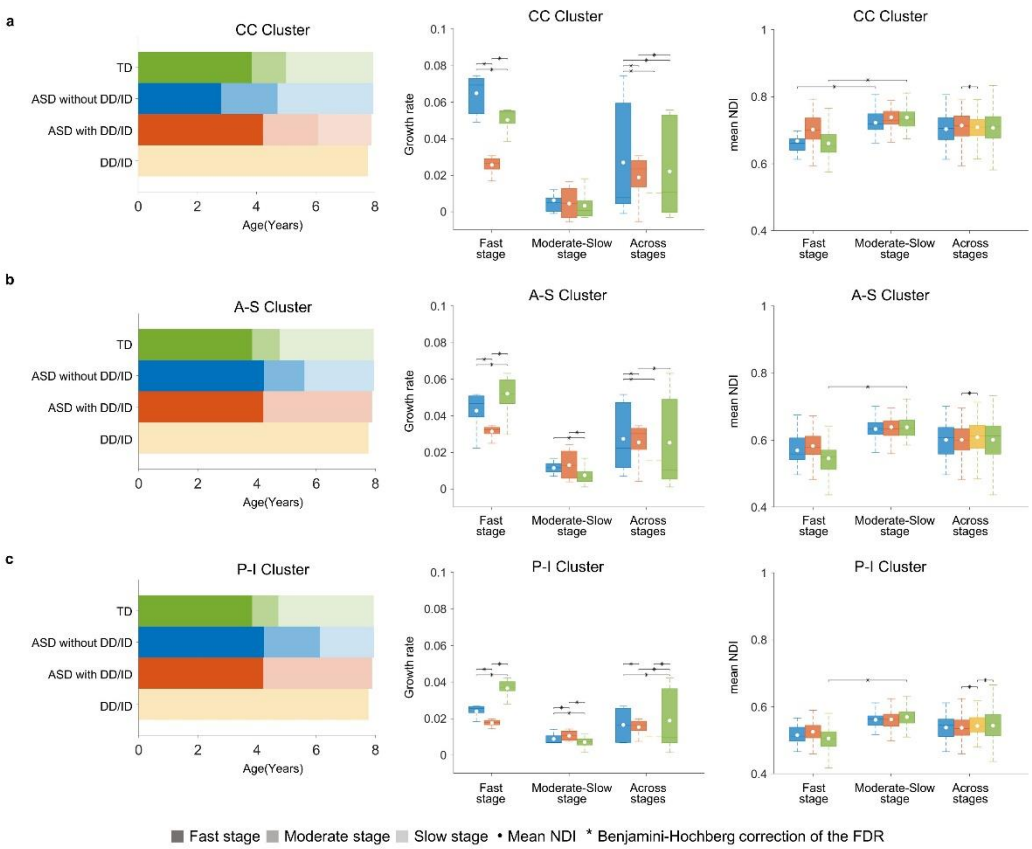

Fig. 5 Associations between the NDI of white matter clusters and social symptoms and cognitive performance in children with ASD. a, during the fast stage, the ASD with DD/ID group showed negative correlations between the NDI and DQ (measuring cognitive capacity and assessed by the Gesell Developmental Schedules (GDS)). The NDI in the A-S cluster was negatively correlated with the fine motor DQ (r=-0.443, P=0.008). The NDI in the P-I cluster was negatively correlated with the adaptive DQ (r=-0.343, P=0.006) and average DQ (r=-0.313, P=0.012). **b**, During the moderate-slow stage, the NDI of the CC cluster in the ASD without DD/ID group was negatively correlated with the scores of social deficits measured by the Social Awareness of Social Responsiveness Scale (SRS) (r=-0.565, P=0.006). Across the entire age range, the ASD without DD/ID group showed a negative correlation between the NDI in the CC cluster and the restricted, repetitive behavior calibrated severity score (RRB_CSS) of the Autism Diagnostic Observation Schedule (ADOS) (r=-0.370, P=0.011). The intelligence quotient (IQ) was measured by the Wechsler Preschool and Primary Scale of Intelligence (WPPSI) and Wechsler Intelligence Scale for Children-Revised (WISC-R). CARS, Childhood Autism Rating Scale. Note that age, sex and head motion were included as covariates. False discovery rate (FDR) correction with Benjamini-Hochberg procedure for multiple comparisons, P<0.05.